


RESEARCH ARTICLE

Post-installation adaptation of offshore wind turbine controls

Emil Smilden^{1,2}  | Stian H. Sørum¹ | Erin E. Bachynski¹  | Asgeir J. Sørensen¹ |
Jørgen Amdahl¹

¹Centre for Autonomous Marine Operations and Systems (NTNU AMOS), Department of Marine Technology, Norwegian University of Science and Technology, Trondheim, Norway
²Equinor Research Center, Equinor ASA, Trondheim, Norway

Correspondence

Emil Smilden, Centre for Autonomous Marine Operations and Systems (NTNU AMOS), Department of Marine Technology, Norwegian University of Science and Technology, Trondheim, Norway.
Email: emil.smilden@ntnu.no

Funding information

Norges Forskningsråd, Grant/Award Number: 223254

Abstract

The cost of offshore wind energy can be reduced by incorporating control strategies to reduce the support structures' load effects into the structural design process. While effective in reducing the cost of support structures, load-reducing controls produce potentially costly side effects in other wind turbine components and subsystems. This paper proposes a methodology to mitigate these side effects at the wind farm level. The interaction between the foundation and the surrounding soil is a major source of uncertainty in estimating the safety margins of support structures. The safety margins are generally closely correlated with the modal properties (natural frequencies, damping ratios). This admits the possibility of using modal identification techniques to reassess the structural safety after installing and commissioning the wind farm. Since design standards require conservative design margins, the post-installation safety assessment is likely to reveal better than expected structural safety performance. Thus, if load-reducing controls have been adopted in the structural design process, it is likely permissible to reduce the use of these during actual operation. Here, the probabilistic outcome of such a two-stage controls adaptation is analyzed. The analysis considers the structural design of a 10 MW monopile offshore wind turbine under uncertainty in the site-specific soil conditions. Two control strategies are considered in separate analyses: (a) tower feedback control to increase the support structure's fatigue life and (b) peak shaving to increase the support structure's serviceability capacity. The results show that a post-installation adaptation can reduce the farm-level side-effects of load-reducing controls by up to an order of magnitude.

KEYWORDS

control design, geotechnical design, offshore wind energy, structural design, structural health monitoring, structural reliability

1 | INTRODUCTION

Support structures are a major contributor to the cost of offshore wind energy. Favored for their cost-efficiency, monopile foundations are prevalent in the European offshore wind industry.¹ The support structures' dimensions are governed by requirements regarding ultimate, serviceability, and fatigue limit states. The environmental load effects in these limit states depend on the wind turbine's control system. It is widely recognized that the fatigue load effects are governed by the global response characteristics which, in turn, depend on the turbine's closed loop properties. Furthermore, the ultimate and serviceability load effects depend on the turbine's operational settings, such as the cut-out and rated wind speed. A number of control strategies are available for reducing load effects in offshore wind turbine (OWT) support structures.²⁻⁷ However, regardless of the control strategy used, there are unavoidable adverse side-effects, such as wear and tear of various wind turbine components, and power output degradation in terms of both quality and quantity.^{2,7} These side-effects may significantly reduce or even offset the cost savings enabled by the load-reducing controls.

The peer review history for this article is available at <https://publons.com/publon/10.1002/we.2467>

This is an open access article under the terms of the Creative Commons Attribution License, which permits use, distribution and reproduction in any medium, provided the original work is properly cited.

© 2020 The Authors. Wind Energy published by John Wiley & Sons Ltd

The interaction between the foundation and the surrounding soil is a major source of uncertainty in estimating the safety margins of support structures.⁸⁻¹⁴ In particular, uncertainty in the support structures' fundamental natural frequency presents a challenge in estimating their fatigue life. The fundamental natural frequency is usually placed in the relatively narrow "soft-stiff" frequency range in between the rotor frequency (1P) and blade passing frequency (3P).¹⁵ Any coincidence with the rotor excitation frequencies may cause a significant reduction in fatigue life. Furthermore, due to increasing turbine sizes, the "soft-stiff" frequency range is falling closer to the wave excitation frequencies, thus making fatigue life estimation even more sensitive to uncertainty in the fundamental natural frequency. There is also uncertainty about the magnitude of responses. This affects not only the estimation of fatigue life but also the estimation of serviceability capacities which are defined in terms of deflections and rotations (tilt) at the pile head and nacelle level.^{16,17} The fatigue and serviceability requirements usually lead to conservative ultimate capacities.¹⁷ Moreover, since structural collapse is caused by failure of the foundation rather than the the surrounding soil, the ultimate capacities are not very sensitive to uncertainties in the soil-structure properties.¹⁸

Although not yet in widespread commercial use, there are many examples of structural monitoring systems having been successfully employed to estimate the modal properties of OWT support structures.¹⁹⁻²⁷ Structural health monitoring has typically been proposed to enable improved life-cycle maintenance and inspection management and early detection of deterioration phenomena, such as scouring around the foundation. The data collected from such monitoring systems could also be useful for making turbine-specific adjustments to the controls. Supposing that information about the true modal properties is available, the uncertainty in the structural safety margins is reduced. Since design standards generally require conservative design margins, the true modal properties are likely to reveal better than expected structural safety performance. Thus, if load-reducing controls have been adopted in the structural design process, it is likely permissible to reduce the use of these during actual operation. This fact can be exploited by incorporating a post-installation adaptation of load-reducing controls into the structural design process. For the majority of turbines, this would lead to a win-win situation where load-reducing controls have been used to reduce the support structure's cost without having to be used in actual operation, at least not to their fullest potential.

The main contribution of this paper is to propose and analyze a post-installation adaptation of control strategies for reducing the cost of OWT support structures. The overall objective is to increase the cost-efficiency of load-reducing controls by mitigating their adverse side-effects at the wind farm level. Hence, the focus is on optimizing the use of existing control strategies rather than the development of new or improved control strategies. A simulation study considering the structural design of a 10 MW monopile OWT under uncertainty in the site-specific soil conditions is conducted in order to evaluate the proposed methodology. Two control strategies are considered in separate analyses: (a) tower feedback control to increase the support structure's fatigue life and (b) peak shaving to increase the support structure's serviceability capacity. The analyses are performed using the aero-hydro-servo-elastic simulation tool SIMA by SINTEF Ocean.

The paper is organized as follows: First, the controls adaptation procedure is formulated as a two-stage design problem in Section 2. Next, the random field soil model and the soil-structure interaction model are presented in Section 3. Further, the simulation setup is described in Section 4. Then, the selection of characteristic soil properties are discussed in Section 5. Finally, the probabilistic outcomes of the two-stage controls adaptation are analysed in Sections 6 and 7, before the paper is concluded in Section 8.

2 | BACKGROUND AND PROBLEM FORMULATION

The structural design of an OWT is a partially iterative process, involving both the wind turbine manufacturer and foundation designer.^{18,28,29} While the support structures' dimensions are determined through an iterative process, current offshore wind projects use standard off-the-shelf rotor-nacelle assemblies that offer limited possibilities for project-specific adaptations. A preliminary design for the rotor-nacelle assemblies (RNA), including the controls, is decided upon in the early stages of the conceptual design phase. The suitability of the rotor-nacelle assemblies is then reassessed on the basis of the actual project-specific data during certification at the end of the structural design process.²⁹ Fischer et al²⁹ demonstrated how the conventional design process can be modified to accommodate the adaptation of control strategies to reduce the cost of support structures. As illustrated in Figure 1, the methodology proposed in the present paper extends the adaptation of load reducing controls to a two-stage design problem.³⁰ In the first stage, the support structures's dimensions and initial settings for the load reducing controls are chosen based on prior information about the uncertain parameters. In the second stage, once more information become available regarding the uncertain parameters, the settings for the load reducing controls are adjusted based on updated estimates of structural safety margins. A two-stage formulation is applicable to design problems for which the uncertainties are related to manufacturing, fabrication, and construction, such as uncertainty in the site-specific soil conditions, or certain structural parameters. In the case of temporal uncertainties, such as the environmental conditions, turbine availability, or soil erosion and degradation, a multi-stage formulation is required for describing the design problem.

A general formulation of the two-stage design problem is given by

$$\begin{aligned} \text{Minimize : } & C_s(x) + E_{\xi}[C_c(x, \xi)] \\ \text{subject to : } & P[G_j(x, \xi) \leq 0] \leq P_j, \quad j = 1, 2, \dots, m \end{aligned} \quad (1)$$

where $C_c(x, \xi)$ is the solution of the second stage problem

$$\begin{aligned} \text{Minimize : } & C_c(x, y(\xi)) \\ \text{subject to : } & P[G_j(x, y(\xi)) \leq 0] \leq P_j, \quad j = 1, 2, \dots, m. \end{aligned} \quad (2)$$

The first stage decision variables $x \in X$ governs the support structure's dimensions and the initial settings for the load reducing controls. The random variables ξ are the uncertain data, which in the present case are parameters related to the soil conditions. The objective of the first stage

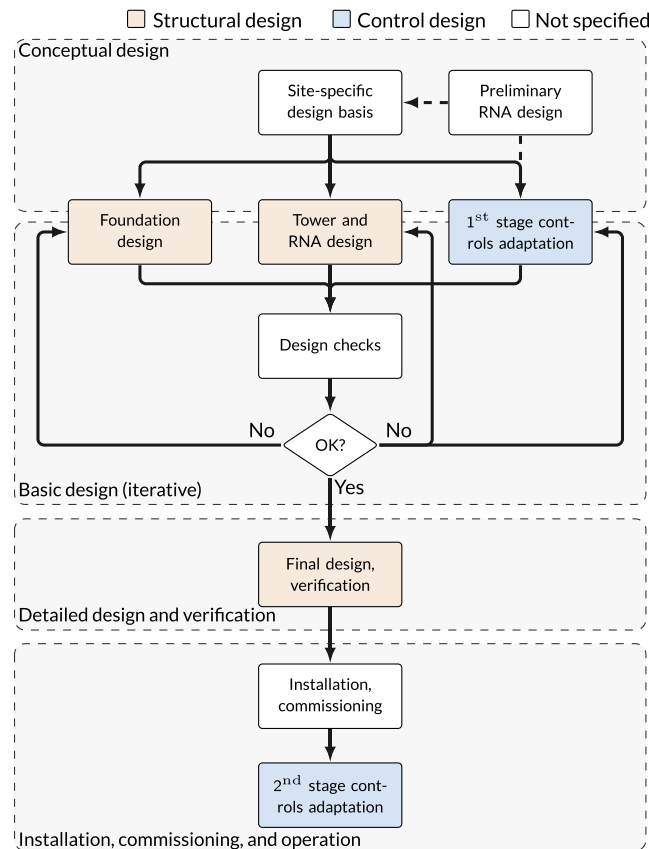


FIGURE 1 Outline of the design process for an offshore wind turbine with a two-stage adaptation of load reducing controls. The outline is based on information presented by Seidel et al,^{18,28} Fischer et al,²⁹ and IEC 61400-3³¹

problem is to minimize the total of the support structure's cost $C_S(x)$ and the expected cost of the control strategies adopted to reduce the support structure's load effects $E[C_C(x, \xi)]$. The dimensions of the support structure are constrained by the probabilities of failure $P[G_j(x, \xi) \leq 0]$ which cannot exceed the target failure probabilities P_j . The required margin of safety must be fulfilled for all failure modes $j = 1, 2, \dots, m$. The second stage decision variables $y \in Y$ govern the settings for the load reducing controls once the uncertain variables have unfolded. The objective of the second stage problem is to minimize the use of load reducing controls, while adhering to the required level of structural safety. The key feature of the two-stage formulation is the interdependence between the first- and second stage in the design problem. Most importantly, in the first stage, decisions should be made taking into account the probabilistic outcome of the second stage problem. Of course, the solution of the second stage problem depends on the decisions made in the first stage.

The two-stage controller adaptation presupposes that information about the true modal properties becomes available once the turbines have been installed. There are several examples where modal identification techniques have been successfully applied to wind turbines.¹⁹⁻²⁷ The modal properties are usually estimated from acceleration data collected at one or more vertical locations along the support structure. Collecting acceleration data at several vertical locations makes it possible to estimate the mode shapes in addition to the modal frequencies and damping ratios.²³⁻²⁵ Reassessing the structural safety margins requires accurate and reliable information about the modal properties. In general, the modal properties estimated at discrete time instants, for instance, during rotor-stop events, are subject to considerable uncertainties.^{20,23,26,27} A system for continuous monitoring should therefore be employed.²⁰⁻²⁵ An example of such a monitoring system was developed and tested in full scale by Devriendt et al.²⁴ Based on data collected from an idling turbine over a 2-week period, the modal properties of five fundamental modes were identified. The applicability of the system was further proven by Weijtjens et al²⁵ who employed data collected over a 2-year period to track changes in the modal frequencies. As further explained in Section 3, the present work considers only uncertainty in the modal frequencies due to the inherent variability in the site-specific soil conditions. It is generally more difficult to obtain accurate and reliable information about the damping ratios than the modal frequencies. Furthermore, in order for the proposed methodology to be presented in a straightforward manner, it is desirable to deal with only one uncertain parameter.

3 | GEOTECHNICAL MODELS

A geotechnical design basis is established in the following. First, the different sources of geotechnical uncertainties are discussed, and the procedure for generating random soil profiles is presented. Then, a random field model is constructed based on conditions at the Dogger Bank in the North Sea. Finally, the soil-structure interaction model is presented.

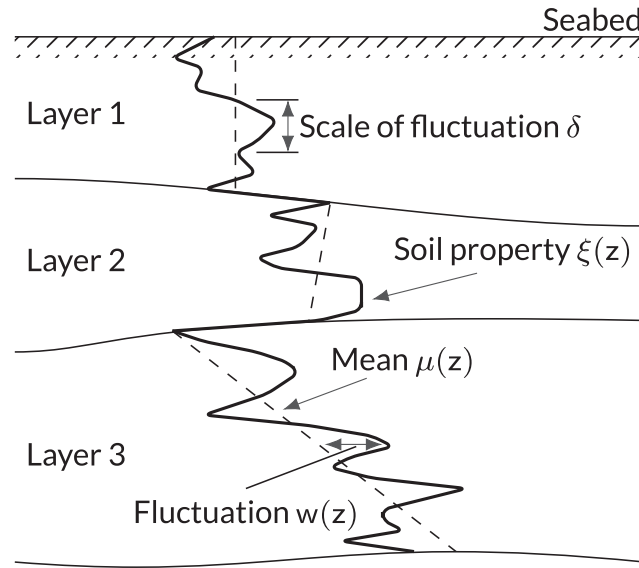


FIGURE 2 Random field model (adapted from Phoon and Kulhawy³²)

3.1 | Geotechnical uncertainties and random field modeling

Soil is a heterogeneous material with properties that vary vertically and horizontally. The three primary sources of geotechnical uncertainty are inherent variability, measurement uncertainty, and transformation uncertainty.^{32–35} The inherent variability of the soil properties is due to natural heterogeneity resulting from continuous geological processes. In general, this source of uncertainty cannot be reduced by collecting more data or performing more tests.³⁵ Measurement and transformation uncertainties emerge from measurement errors, statistical uncertainty due to limited amounts of information, and the correlation models used for transforming field or laboratory measurements into engineering properties. These uncertainties depend on the quality of the equipment being used, procedural control, and the amount of data collected.^{32,35} In practice, the uncertainties due to measurement and transformation errors are often embedded in the inherent variability under the assumption that their contributions to the overall uncertainty are small.³⁵ Furthermore, depending on the number of samples, the statistical uncertainty can be taken into account in the estimation of the soil properties' mean value.³⁵ Hence, only the inherent soil variability is modeled in the present work.

Inherent soil variability is usually modeled as random fields characterized by their mean, coefficient of variation (COV), and scale of fluctuation.^{32–34} As illustrated in Figure 2, the spatial variability of a soil property ξ can be decomposed into a mean trend μ and a fluctuating component w , such that

$$\xi(z) = \mu(z) + w(z) \quad (3)$$

where z is the depth below the ground surface.³² Within a soil layer, the mean trend is often assumed either constant, or linearly varying with depth. The vertical scale of fluctuation δ is the distance over which the soil property shows strong correlation. The distance δ is related to the average distance between crossings of the fluctuating soil property and the mean trend.^{32,34}

It is straightforward to generate a vertical sequence of correlated random soil properties from a random field with probability distribution $F_{\xi}(\xi)$.^{10,12,36} For each random field realization, a vector \mathbf{U} of uncorrelated standard Gaussian distributed variables U_i where $i = 1, 2, \dots, n$ is generated. The dimension n corresponds to the number of depth increments in the soil-structure interaction model. The vector \mathbf{Y} of correlated standard Gaussian distributed variables Y_i is then computed by Choleski triangulation of the positive definite correlation matrix ρ , such that

$$\mathbf{Y} = \mathbf{T}\mathbf{U}, \quad \mathbf{T}\mathbf{T}^T = \rho \quad (4)$$

where \mathbf{T} is the lower triangular matrix. The correlation matrix describes the vertical correlation structure of the random field, which is frequently characterized by autocorrelation functions. Such functions describe the correlation between two points based on their vertical separation distance (lag) and the vertical scale of fluctuation.³⁴ Finally, the vertical sequence ξ of correlated random soil properties ξ_i can be computed by applying the componentwise transformation given by

$$\xi_i = F_{\xi}^{-1}(\Phi(Y_i)), \quad i = 1, 2, \dots, n \quad (5)$$

where $\Phi(Y_i)$ is the standard Gaussian probability distribution.

3.2 | Random field model

A wind farm site at the Dogger Bank in the North Sea is used as a basis for establishing the random field model. The soil profile at the design location consists of a surface layer of dense sand with underlying layers of stiff clays. Based on these soil conditions, a simple three-layered

TABLE 1 The three-layered random field model

Layer	Depth Range, m	Type	Soil Property	Distribution	Mean $\mu(z)$	COV, %	Scale of Fluctuation δ , m
1	0-5	Dense sand	Friction angle ϕ , deg	Normal	40	15	0.5/2.0/5.0
			Submerged unit weight γ , kN/m ³	Deterministic	10	0	∞
2	5-15	Stiff clay	Undrained shear strength s_u , kPa	Lognormal	75	40	1.0/5.0/10.0
			Submerged unit weight γ , kN/m ³	Deterministic	10	0	∞
3	15-38	Stiff clay	Undrained shear strength s_u , kPa	Lognormal	$75 + 3(z - 15)$	40	1.0/5.0/10.0
			Submerged unit weight γ , kN/m ³	Deterministic	10	0	∞

Note. The coefficients of variation and vertical scales of fluctuation are based on the guidelines for typical soil property variability by Phoon and Kulhawy.^{32,33} The correlation lengths in bold are used in the analysis of the two-stage controls adaptation.

random field model is constructed. For geotechnical design in clay, the submerged unit weight γ and undrained shear strength s_u are typical parameters used to describe the mechanical behavior of soil. Likewise, the mechanical behavior of sand is described by the submerged unit weight and angle of internal friction ϕ . Under the assumption of low variability, the submerged unit weight is treated as a deterministic parameter.^{32,33} Thus, only the undrained shear strength and the angle of internal friction are modeled as random fields.

The random field model is defined in Table 1. In the surface layer of sand, the mean and standard deviation of the random field are assumed independent of depth. In the underlying layers of clay, the mean and standard deviation are assumed independent of depth in the upper layer, and linearly increasing with depth in the lower layer. The coefficients of variation and vertical scales of fluctuation are selected based on the guidelines for soil property variability by Phoon and Kulhawy.^{32,33} Here, the angle of internal friction is assumed normally distributed.³⁵ Accordingly, the componentwise transformation $Y_i \rightarrow \phi_i$ for the angle of internal friction is given by

$$\phi_i = \mu_i + \sigma_i Y_i, \quad i = 1, 2, \dots, n \quad (6)$$

where μ_i and σ_i are the means and standard deviations in the n depth decrements in the surface layer of sand. The undrained shear strength is assumed lognormally distributed in the present work. The shear strength of clay stems from the sum of frictional resistance between soil particles, which under the central limit theorem implies that the shear strength is asymptotically normally distributed.³⁷ Nevertheless, in order to avoid unphysical negative values, the undrained shear strength is usually modeled as a lognormally distributed variable.³⁵ The componentwise transformation $Y_i \rightarrow s_{u,j}$ for the undrained shear strength is given by

$$s_{u,j} = \exp(\mu_{ln,j} + \sigma_{ln,j} Y_i), \quad i = 1, 2, \dots, m \quad (7)$$

where $\mu_{ln,j}$ and $\sigma_{ln,j}$ are the lognormal mean and standard deviation in the m depth decrements in the underlying clay layers.

The vertical autocorrelation structure of the random fields is assumed to follow an exponential decay model as described by Vanmarcke.³⁴ Accordingly, the correlation ρ between two points separated by a distance $\tau_{ij} = z_i - z_j$ is given by

$$\rho_{ij} = \exp\left(-\frac{2|z_i - z_j|}{\delta}\right), \quad i = 1, 2, \dots, p, \quad j = 1, 2, \dots, p \quad (8)$$

where p is the number depth decrements in the respective soil layers. There is no correlation between the upper layer of sand and the underlying layers of clay.

3.3 | Soil-structure interaction model

Laterally loaded piles, such as OWT monopile foundations, are often designed using the so-called p-y method, according to the recommended practice issued by the American Petroleum Institute (API).³⁸ In accordance with Winkler's foundation model, the lateral interaction between the foundation and the surrounding soil is described by a series of uncoupled nonlinear springs. A set of p-y curves describes the nonlinear relationship between lateral displacement y and soil resistance p . The appropriate choice of p-y curves depends on the type of soil and whether the pile is subjected to static, dynamic, or cyclic loading.^{38,39} For piles in sand, the standards DNV-OS-J101³⁹ and API-RP-2GEO³⁸ recommend the p-y curves proposed by Murchison and O'Neill.⁴⁰ For piles in clay, the standards unanimously recommend the p-y curves proposed by Matlock⁴¹ for soft clays, while API-RP-2GEO recommends the p-y curves proposed by Reese and Welch⁴² for stiff clays. The present work uses the p-y curves of Murchison and O'Neill⁴⁰ for modeling the upper sand layer, and the p-y curves of Matlock⁴¹ for modeling the underlying clay layers. Corrections for cyclic loading are applied in accordance with DNV-OS-J101.³⁹

While the standards consistently recommend application of the p-y method, there are several known shortcomings to this modeling approach. Without exception, the p-y curves are derived from field tests performed on flexible piles with length to diameter ratios well above those of OWT monopile foundations.^{11,13} Furthermore, while the p-y curves include corrections for cyclic loading, these are calibrated based on field data collected from piles subjected to a low number of loading cycles compared with the cycle count over the service life of an OWT.^{11,13} The

implications of these and other shortcomings of the p-y method are widely discussed in the literature on geotechnical modeling for OWTs.^{8,9,11,13,14} Although soil-structure modeling errors are a significant source of uncertainty, this is not taken into account here. First of all, there are currently no statistical models available capable of reasonably capturing this uncertainty. Furthermore, Damgaard et al¹¹ estimated the fundamental bending frequencies of 54 OWTs based on 510 free vibration tests. Their results showed that the p-y method consistently underestimated the fundamental bending frequencies compared with the full-scale measurements. Thus, neglecting soil-structure modeling uncertainty is expected to yield conservative safety margins for the support structure. Since the difference between design and reality will be larger in practice, the present study presents a conservative estimate of the effectiveness of the proposed methodology in reducing the farm-level side-effects of load-reducing controls.

4 | SIMULATION SETUP

The simulation setup is described in the following. First, the simulation model is described. Then, the procedure for the fatigue life analysis is presented, including design load cases and environmental load cases. Finally, the procedure for the serviceability analysis is established, including the estimation of 1-year loading conditions.

4.1 | Simulation model

The OWT model is based on the DTU Wind Energy 10MW reference turbine⁴³ which is placed on a monopile foundation with diameter 8.5 m. The water depth is 25 m, and the penetration depth of the monopile is 38 m below the seabed. Monopile dimensions (diameter, thickness, penetration depth) are selected based on considerations regarding natural frequencies, fatigue life, and overall loading levels. Basic control functions (baseline controls) are implemented based on the DTU Wind Energy controller.⁴⁴ Simulations are performed using the aero-hydro-servo-elastic software tool SIMA by SINTEF Ocean. In SIMA, the structural components are modeled using nonlinear beam elements which account for large deformations and nonlinear geometrical stiffness. Morison's equation and Airy linear wave theory are used to model the hydrodynamic loads. The wave kinematics are integrated to the instantaneous free surface and the drag- and mass coefficients are taken as $C_D = 0.9$ and $C_M = 2.0$, respectively.⁴⁵ Blade element momentum theory is used to model the aerodynamic loads. Appropriate corrections for dynamic inflow, skewed inflow, dynamic wake, tower shadow, tip loss, and hub loss are included in the aerodynamic load model.⁴⁶ The JONSWAP spectrum with peak enhancement factor given by the standard DNV-RP-C205⁴⁷ is used to generate wave time series in SIMA. The Kaimal spectrum with exponential coherence model is used to generate three-dimensional wind fields using NREL's Turbsim.⁴⁸

Stiffness-proportional Rayleigh damping is used to take into account material, hydrodynamic, and soil-structure damping. The damping ratio of the fundamental bending mode is taken as 1.1% where 0.5% is attributed to the material and hydrodynamic damping, and the remaining 0.6% is attributed to the soil-structure interaction. The material and hydrodynamic damping is applied in all segments of the support structure while the soil-structure damping is applied only in the foundation beneath the mudline. In addition to the structural damping, the support structure is equipped with two tuned mass dampers, weighing 20 tonnes each. These damping devices are mounted in a perpendicular configuration in the tower beneath the nacelle. When the dampers are tuned to the first fore-aft natural frequency they increase the damping ratio of the fundamental bending mode by approximately 1.1%.

4.2 | Fatigue life analysis

The lifetime accumulation of fatigue damage in OWT support structures is usually estimated from a limited number of short-term time domain simulations. In order to reduce the computational effort, metocean data are lumped into environmental load cases. The number and resolution of these environmental load cases must be sufficient to capture the fatigue contributions from the full long-term distribution of the environmental parameters.⁴⁹ Furthermore, design standards such as DNV-ST-49 require the consideration of design load cases covering all relevant combinations of environmental conditions (wind, wave, ice), operating states (power production, idling, parked, start-up, shut-down, fault occurrences), and accidental states (ship collision, fire).

A reduced set of design load cases is considered in the present work. The design load cases, summarized in Table 2, cover only the loading conditions which contribute substantially to the lifetime accumulation of fatigue damage in the support structure. In accordance with the standard DNV-ST-49 a conservative 90% availability is assumed for the turbine. The incidence of unavailability is an important consideration in estimating

TABLE 2 The reduced set of design load cases used for estimating the lifetime utilization of fatigue damage in the support structure⁷

DLC	Design Situation	Description
1.2	Power production	Normal operation without faults
6.4	Idling	Idling outside the normal operating range
7.2	Parked with fault	Parked/Idling with fault

Note. The design load cases are defined in accordance with the standard DNV-ST-0437.⁴⁹

TABLE 3 The reduced set of environmental load cases used for estimating the serviceability utilization of the support structure

Loading Condition	Environmental Parameters		
	V, m/s	H_s , m	T_z , s
One-year peak loading in rated conditions	11.0	4.3	7.0
One-year peak loading in cut-out conditions	25.0	7.6	9.7

Note. The environmental load cases cover the mean wind speed V , significant wave height H_s , and wave zero-crossing period T_z .

the fatigue life of OWT support structures. Since the aerodynamic damping is negligible when the rotor is at standstill, unavailability occurrences lead to a significant increase of wave-induced fatigue load effects.^{2,7} The effect of unavailability on the fatigue life can be reduced by so-called active idling.^{2,7} When the turbine is in active idling, the blades are pitched only partly into the wind, causing the rotor to rotate at low speed and hence produce aerodynamic damping. Here, the turbine is assumed capable of active idling 75% of the time it is unavailable following the discussion by Smilden et al.⁷ While it has yet to become standard practice, active idling presents a promising cost reduction measure for future generations of offshore wind turbines.

The environmental loads cases are established following the procedure described by Smilden et al.⁷ Metocean data for a wind farm site at the Dogger Bank in the North Sea are obtained from a hindcast carried out by the Norwegian Meteorological Institute.⁵⁰ Fatigue equivalent environmental load cases are constructed from the metocean data based on the long-term distribution of fatigue damage. The environmental load cases cover the mean wind speed, significant wave height, wave peak period, and the wind/wave misalignment. The turbulence and the wind shear are accounted for in accordance with IEC 61400-1,⁵¹ assuming Class B normal turbulence conditions. For each environmental load case, time domain simulations with a total duration of 3600 seconds are performed.

4.3 | Serviceability analysis

The serviceability limit state ensures that the deflections and deformations of the support structure during normal operation do not exceed the tolerances for which the turbine can operate safely. For monopile OWTs, the serviceability criteria are often defined in terms of deflections and rotations (tilt) at the pile head and nacelle level, including both the initial tilt after installation and permanent rotation accumulated over the turbine's service life.^{9,17} The rotational requirements are usually the main concern as overturning moments are of greater importance than the horizontal forces.¹⁷ Further, since the rotations at the pile head and nacelle level are closely related, the serviceability capacity of the support structure may be expressed in terms of pile head rotation.¹⁶ Recommendations for the permissible pile head rotation are given in design standards such as DNV-OS-J101.³⁹ The tolerance for the total rotation is often on the order of 0.5°, allowing for an initial rotation of 0.25° after installation and 0.25° permanent accumulated rotation. Evaluation of the initial rotation is considered outside the scope of this paper. Hence, the tolerance for the pile head rotation is taken as the remaining 0.25°. There is currently no consensus and furthermore no available guidelines on how to determine permanent accumulated pile rotation. A common and conservative approach is to evaluate the pile rotation under peak loading conditions,^{9,14,17,52} which is the approach adopted here. It is assumed that permanent accumulation of pile rotation occurs during operation when the mean pile rotation is significantly larger than zero. For further discussion on methods for estimating permanent accumulated pile rotation, see Carswell et al.⁹ In accordance with the recommendations of the standard DNV-OS-J101³⁹ for the serviceability limit state, extreme loading conditions with a 1-year return period are used in the analyses.

The peak wind load with a n -year return period is expected to occur in near-rated conditions where the aerodynamic thrust is at its maximum. In contrast, the n -year peak wave load—during power production—is expected to occur in near-cut-out conditions due to the monotonically increasing relationship between wind speed and the significant height of wind-waves. In order to correctly estimate the n -year response, the modified environmental contour method is employed.⁵³ This method is a modification of the widely used environmental contour method.⁵⁴ First, the characteristic wind speeds are selected deterministically as the wind speeds for which the peak wind and wave loads are expected to occur. Then, for each characteristic wind speed, the n -year sea state contour is constructed using Rosenblatt's transformation. In the statistical model, the significant wave height H_s is modeled as dependent on the mean wind speed V while the wave zero-crossing period T_z is modeled as dependent on H_s . In accordance with the standard DNV-ST-49 a three-parameter Weibull distribution is assumed for H_s . Further, the conditional distribution of T_z given H_s is assumed to be lognormal.⁵⁵

The environmental load cases used for estimating the serviceability utilization of the support structure are presented in Table 3. The environmental load cases cover the mean wind speed, significant wave height, and the wave zero-crossing period. Turbulence and wind shear are accounted for in accordance with IEC 61400-1,⁵¹ assuming Class B normal turbulence conditions. Several combinations of environmental parameters should in principle be considered for each loading condition. However, one set of environmental parameters is found sufficient for the analyses performed here. As both wind and waves are random processes, the maximal pile head rotation is a stochastic variable. In order to estimate the serviceability utilization, the maximum pile head rotation must be determined from time series of responses. The expected maximum value of 10 one-hour time series is taken as the maximum pile head rotation.

5 | SELECTING CHARACTERISTIC SOIL PROPERTIES

Analysis of the two-stage controls adaptation requires selecting characteristic soil properties for use in the pre-installation prediction of the structural safety margins. While several researchers have studied the effects of soil-structure uncertainty in a structural reliability context,^{8,10,12,56} there are few publications that deal with the selection of characteristic soil properties.⁵² In general, the appropriate choice of characteristic soil properties depends on the type of support structure and limit state in consideration. According to the standard DNV-OS-J101,³⁹ a tail quantile in soil property distribution should be used if the limit state is governed by a small soil volume. Likewise, the soil property's mean value should be taken as the characteristic value if the limit state is governed by a large soil volume. Furthermore, the characteristic values should be selected as cautious estimates of the values governing the limit state in consideration. The geotechnical design of monopile OWT foundations involves a rather large volume of soil. Consequently, the depth dependent characteristic soil property should be a cautious estimate of the mean trend. The characteristic value ξ_K is typically expressed as the mean minus the standard deviation multiplied with some factor γ_K ,³⁵ such that

$$\xi_{K,i} = \mu_i - \gamma_K \sigma_i, \quad i = 1, 2, \dots, n \quad (9)$$

where μ_i and σ_i are the means and standard deviations at the n depth decrements. The factor γ_K is selected based on the required level of caution.³⁵ Design standards, such as DNV-RP-C207,⁵⁷ provide general guidelines on the selection of γ_K based on the number of observations in the soil layers. These guidelines are appropriate under the assumption of negligible variance in the design-driving soil properties. This is a reasonable assumption for piles under axial loading, for which the soil over the entire embedment length contributes to the load carrying capacity.³⁷ As the following analysis will show, this is not necessarily the case for laterally loaded piles such as monopile OWT foundations.

Figure 3 presents the distribution of the fundamental fore-aft natural period for different vertical scales of fluctuation. Only the fore-aft period is presented here since the fore-aft and side-side bending modes have closely spaced periods with similar distributions. Since the natural periods are bounded from below by those with fixed boundary conditions at the seabed, their distributions are negatively skewed.^{10,11,26} As expected, the variance of the natural period depends on the vertical correlation length. Thus, for limit states that are closely correlated with the natural period, neglecting vertical correlation does not yield a consistent level of safety.

Figure 4 presents the horizontally averaged soil properties for all outcomes of the natural period above the 95%-quantile and below the 5%-quantile. The random field realizations associated with natural periods in the tail quantiles deviate from the mean trend. In general, sand provides greater soil-pile stiffness than clay. The angle of internal friction therefore exhibits larger deviations from its mean value than the undrained shear strength. Furthermore, since the natural periods are governed by the soil-pile stiffness near the seabed and pile toe, larger deviations are observed in the upper and lower depth ranges. It is clear that the natural period is not governed by the entire soil volume, but a combination of the soil volumes near the seabed and pile toe. This needs to be taken into consideration in selecting characteristic soil properties.

Here, the characteristic soil properties are estimated based on the distribution of the natural period. Based on eigenvalue analysis, the factor γ_K is adjusted until the desired level of safety is achieved. Similar to the guidelines for limit states governed by a small soil volume,^{39,57} a 5% margin of safety is adopted. Hence, under the assumption that the fatigue life and serviceability capacity monotonically decrease with increasing natural period, the 95%-quantile is taken as the target natural period in the calibration of γ_K . The resulting factors γ_K are presented in Table 4 together with the means and coefficients of variation for the natural period. Note that there is not necessarily a one-to-one relationship between the fundamental bending frequency and the fatigue life and serviceability capacity. Furthermore, ultimate limit states need also to be considered in practice. It was found through initial analysis work that, for the present study, it was reasonable to make this assumption about the safety margins of the support structure.

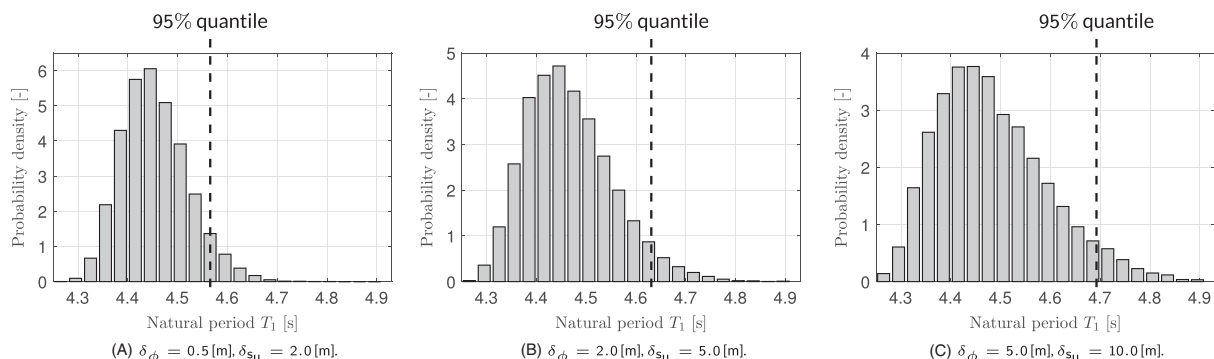


FIGURE 3 The distribution of the support structure's fundamental fore-aft period T_{Δ} resulting from 10 000 random field realizations. Correlation lengths $\delta_{\phi} = 2.0$ and $\delta_{s_u} = 5.0$ [m] are used in the analysis of the two-stage controls adaptation

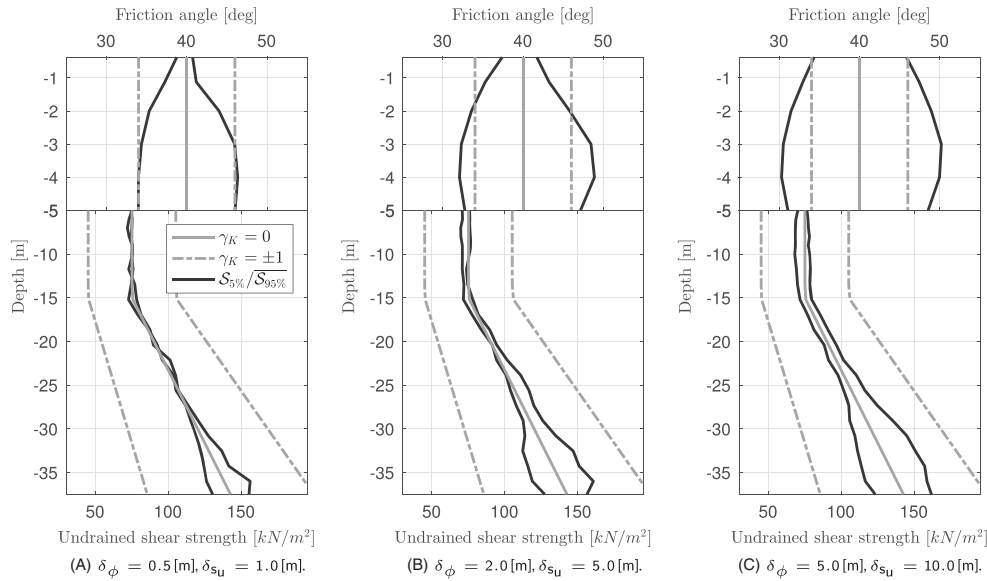


FIGURE 4 Horizontally averaged soil properties for all outcomes of the support structure's fundamental fore-aft period T_{Δ} outside selected tail quantiles in the distribution of T_{Δ} resulting from 10 000 random field realizations. Results are presented for random field realizations resulting in natural periods below the 5%-quantile $S_{II\%}$ and above the 95%-quantile $\overline{S_{95\%}}$. Correlation lengths $\delta_{\phi} = 2.0$ and $\delta_{s_u} = 5.0$ [m] are used in the analysis of the two-stage controls adaptation

TABLE 4 The characteristic soil factor γ_K calibrated to a 5% level of safety based on the distribution of the support structure's fundamental fore-aft period T_1 resulting from 10000 random field realizations. The means and coefficients of variation for the natural period are also presented. Correlation lengths $\delta_{\phi} = 2.0$ and $\delta_{s_u} = 5.0$ [m] are used in the analysis of the two-stage controls adaptation

Scale of Fluctuation		Mean, s	COV, %	T_1 (95% Quantile)	γ_K (95% Quantile)
δ_{ϕ} , m	δ_{s_u} , m				
0.5	1.0	4.45	1.5	4.57	0.42
2.0	5.0	4.47	2.0	4.63	0.65
5.0	10.0	4.48	2.5	4.69	0.86

6 | TWO-STAGE ADAPTATION OF A CONTROL STRATEGY FOR FATIGUE LOAD REDUCTION

The two-stage adaptation of a control strategy capable of increasing the fatigue life of support structures is analysed in the following. First, the lifetime effects of the adopted control strategy are analyzed. Then, tradespace methodology is employed to establish a near-optimal strategy for the second stage controls adaptation. Finally, the probabilistic outcome of the two-stage controls adaptation is analyzed.

6.1 | First-stage controls adaptation

The first stage adaptation of a control strategy capable of increasing the fatigue life of support structures is performed in this section. Only a brief analysis is included here as similar analyses can be found in the literature.^{2,7,29} In the first stage, decisions need to be made regarding what control strategies to adopt to increase the support structure's fatigue life. A number of control strategies are available for this purpose.^{2-5,7} A widely used strategy is to employ collective pitch control to increase the support structure's damping, often referred to as tower feedback control.^{3,4} As collective pitch control only effectively reduces loads parallel to the wind direction, it may also be beneficial to increase the damping in the cross-wind direction by either individual pitch control,² or generator torque control.^{2,3,5} The effectiveness of the various control strategies depends on the type of foundation and the site-specific conditions, such as the water depth and the environmental characteristics.^{2,7}

Here, only collective pitch control is adopted to increase the fatigue life of the support structure. Tower feedback control is implemented via an auxiliary control loop, using the control scheme proposed by Smilden et al.⁵⁸ The control scheme extends conventional tower feedback control to provide both damping and stiffness to the support structure's fore-aft bending modes. The tower feedback control actions β_{TFC} are governed by the following control law:

$$\beta_{\text{TFC}} = -\frac{1}{F_A^{\beta}(\alpha)} (K_P(X - x_{\text{ref}}) + K_D\dot{X}), \quad F_A^{\beta}(\alpha) = \frac{\partial F_A}{\partial \beta} |_{\alpha} < 0, \quad (10)$$

where $K_P \geq 0$ is the proportional (stiffness) gain, and $K_D \geq 0$ is the derivative (damping) gain. The demanded pitch actions are scheduled by the partial derivative from pitch angle to aerodynamic thrust $F_A^{\beta}(\alpha) < 0$ where the vector $\alpha \in \mathbb{R}^{4 \times 1}$ consists of parameters governing the aerodynamic loads. The reference tower displacement trajectory x_{ref} is generated by a reference model which estimates the wind-induced progress of the

TABLE 5 Results for the first stage adaptation of tower feedback control to increase the support structure's fatigue life

Controller Adaptation	Fatigue Utilization		Adverse Side Effects	
	$D_{Max}^{20-year}$, -	$\Delta D_{Max}^{20-year}$, %	$\Delta DEL_{\beta}^{20-year}$, %	ΔDEL_{Shaft}^{20} , %
Baseline control	1.77	0.0	0.0	0.0
Tower feedback control	1.00	-43.5	+25.4	+6.6

Note. Normal operation without tower feedback control is referred to as baseline control. The change in damage equivalent loads for the pitch actuator bearings and main shaft are denoted by $\Delta DEL_{\beta}^{20-year}$ and ΔDEL_{Shaft}^{20} , respectively. Further, the support structure's fatigue utilization and change in fatigue utilization are denoted as $D_{Max}^{20-year}$ and $\Delta D_{Max}^{20-year}$, respectively. A normalization factor of 1.4 is applied to the results in order to achieve the target fatigue utilization ($D_{Max}^{20-year} = 1$) only if tower feedback control is used.

tower displacement. Further, an extended Kalman filter is applied to calculate the required state estimates such as the tower displacement x and the tower velocity \dot{x} . The tower feedback controller is operated with different sets of controller gains depending on the operational mode of the turbine. In the partial load region, only derivative action is used, rendering the control scheme a conventional tower feedback controller. In the full load region, tower feedback control with proportional-derivative action is used.

The additional costs of tower feedback control are primarily related to increased wear of various wind turbine components. In particular, it increases the fatigue loads in the pitch system and drive-train module, including the gearbox assembly.^{7,58} Hence, the damage equivalent loads in the main shaft and pitch actuator bearings are taken as parameters to evaluate the effects of tower feedback control.⁷ The damage equivalent loads in the main shaft are computed from the time histories of the shaft's torsional loading with rainflow counting of stress amplitudes. In the case of the pitch actuator bearings, the fatigue damage is governed by the overturning moments in the actuator and the number of revolutions for the bearing. The load distribution duration method is therefore used to compute the damage equivalent loads in the pitch bearings. For both components, the slope exponent of the S-N curve is taken as 3 in the fatigue calculations.⁷

Table 5 presents the result of the first stage adaptation of tower feedback control. Tower feedback control significantly increases the fatigue life of the support structure. Monopile OWT foundations are typically designed for a fatigue life of 50 years.^{16,17} Moreover, the standard DNV-OS-C101⁵⁹ requires a safety factor of at least 3.0 for offshore steel structures with non-accessible areas. In addition, a normalization factor of 1.4 is applied to the fatigue damage in order to achieve the target fatigue utilization ($D_{Max}^{20-year} = 1$) only if tower feedback control is used. Although there is a slight excess of fatigue life, the dimensions of the foundations are not further optimized. As expected, the fatigue loads in the pitch actuator bearings and the main shaft are increased significantly as a result of the additional pitch activity.

Figure 5 presents the fatigue utilization of the support structure with and without tower feedback control. The maximum fatigue utilization occurs in the cross-section located 4 m below the seabed. In this cross-section, the maximum fatigue utilization occurs in the southwest/northeast direction due to a high incidence of wind and wind-generated sea from southwest.⁶⁰

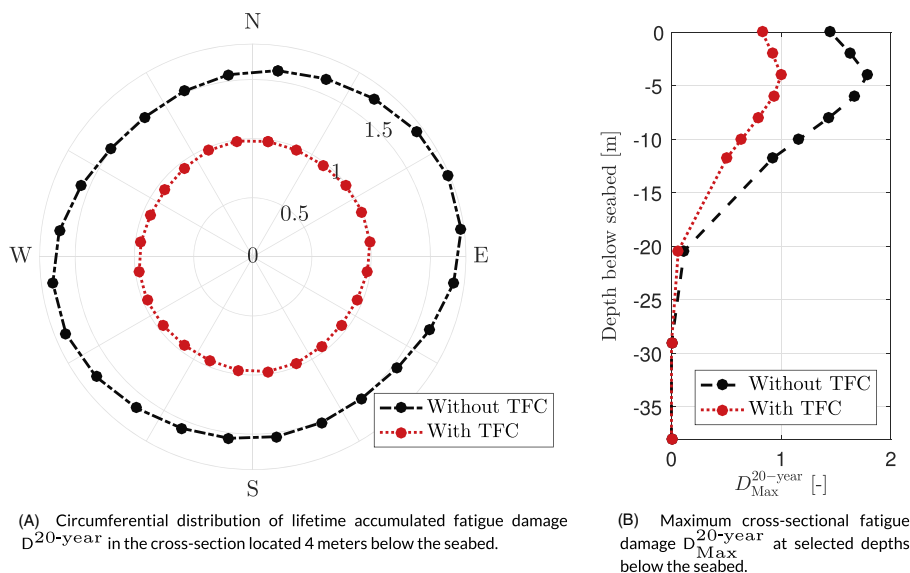


FIGURE 5 Results for the first stage adaptation of tower feedback control (TFC). Normal operation without tower feedback control is referred to as baseline control (baseline). A normalization factor of 1.4 is applied to the results in order to achieve the target fatigue utilization ($D_{Max}^{20-year} = 1$) only if tower feedback control is used

6.2 | Second-stage controls adaptation

The procedure for the second stage adaptation of tower feedback control is established in this section. In the second stage, the aim is to reduce as much as possible the use of tower feedback control while still adhering to the required level of structural safety. The second-stage controls adaptation should be performed in a way that minimizes complexity and that leads to minimal adverse side-effects. A practical way of achieving these objectives is to limit the use of tower feedback control to specific environmental conditions, here referred to as event-triggered tower feedback control.^{7,61,62} The best choice of trigger criteria depends on the control strategy being used and how its desirable and undesirable effects are prioritized.^{7,61,62} First, the triggering environmental parameters must be selected. It could be possible to collect information about the sea state from a nearby wave buoy or a wave radar.²⁵ Still, access to reliable and accurate estimates of the sea state parameters is a requirement that might be difficult to fulfill. Moreover, in order to avoid chattering between different operating modes, it is desirable to limit the number of triggering parameters. The mean wind speed is therefore taken as the only triggering parameter in the present work. Further, the wind speed criteria for triggering tower feedback control are established using tradespace exploration as described by Smilden et al.⁷

It is unnecessary to perform a lifetime fatigue analysis for each combination of trigger criteria. Instead, a post-processing algorithm is applied to compute the lifetime effects of temporarily enabled tower feedback control.⁷ First, lifetime fatigue analyses are carried out with and without tower feedback control. Then, the results from two analyses are merged in combinations corresponding to different trigger criteria. In total, 2048 combinations of trigger criteria are possible from the grouping of the metocean data.

The tradespaces for event-triggered tower feedback control are presented in Figure 6. The effects of tower feedback control, both desirable and undesirable, are sensitive to the soil conditions. This is expected as the magnitude of the support structure response depends on the global stiffness and the degree to which the fundamental bending mode is excited. The scenarios with a single trigger criterion are highlighted in the tradespaces. With respect to the pitch actuators, it is optimal to use trigger criteria of the type $V_{TFC} \geq V_{TFC}^{Lim}$, meaning that tower feedback control is used for wind speeds above V_{TFC}^{Lim} . Notably, the opposite trend is observed for the main shaft, for which trigger criteria of the type $V_{TFC} \leq V_{TFC}^{Lim}$ are close to optimal. It is clear that the best choice of trigger criteria depends on the priority of the adversely affected components. However, the tradespaces reveal general patterns independent of the site-specific soil conditions. With regard to the second stage controls adaptation, it is therefore reasonable to define a single set of trigger criteria. Here, the pitch actuators are given priority and trigger criteria of the type $V_{TFC} \geq V_{TFC}^{Lim}$ are used.

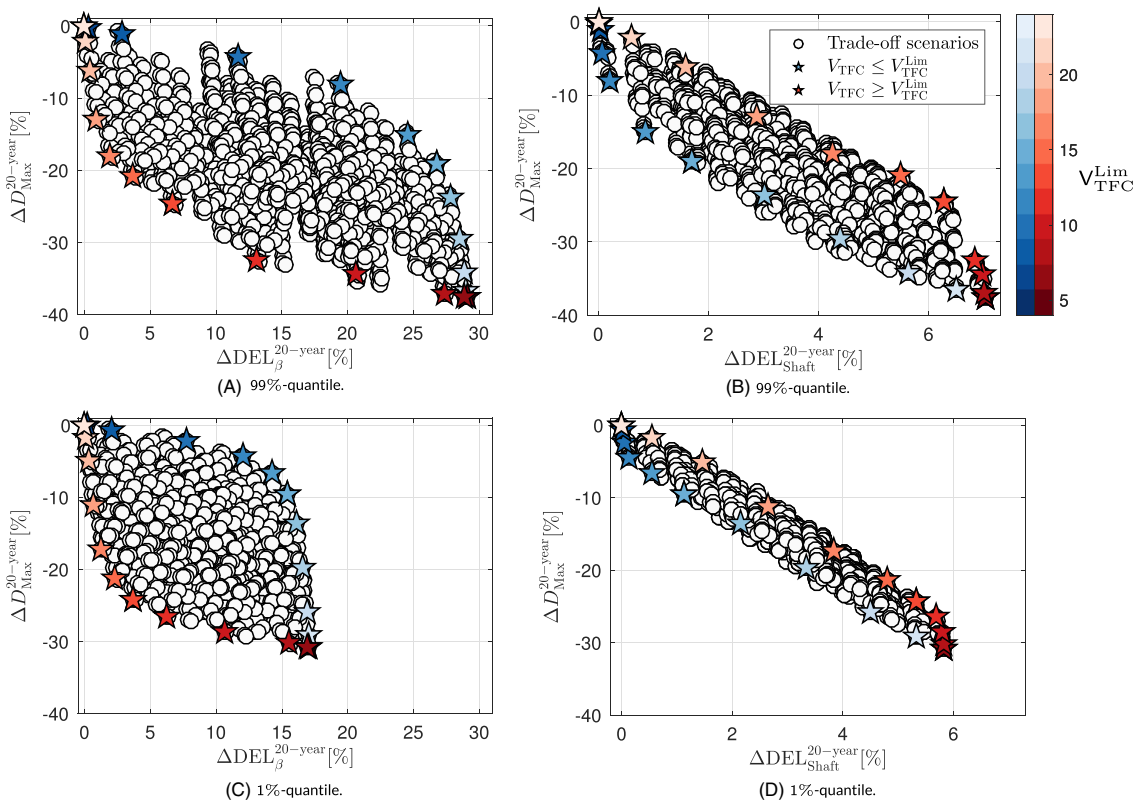


FIGURE 6 Tradespaces used for establishing the procedure for the second stage adaptation of tower feedback control. The tradespaces are constructed by considering event-triggered tower feedback control with mean wind speed as the triggering parameter. Results are presented for characteristic soil properties corresponding to 1% and 99% quantiles in the distribution of the natural period T_{Δ} . The change in damage equivalent loads for the pitch actuator bearings and main shaft are denoted by $\Delta DEL_{\beta}^{20\text{-year}}$ and $\Delta DEL_{\text{Shaft}}^{20\text{-year}}$, respectively. Further, $\Delta D_{\text{Max}}^{20\text{-year}}$ denotes the change in fatigue utilization for the support structure. The stars highlight the scenarios with a single trigger criterion V_{TFC}^{Lim} . Trigger criteria of the type $V_{TFC} \geq V_{TFC}^{Lim}$ (red stars), meaning that tower feedback control is used for wind speeds greater than V_{TFC}^{Lim} , are adopted for the second stage controls adaptation

6.3 | Probabilistic outcome of the two-stage controls adaptation

The probabilistic outcome of a two-stage adaptation of tower feedback control is analyzed in this section. Monte Carlo methodology is employed to compute the probabilistic outcome of the post-installation adaptation of tower feedback control. First, a set of random field realizations is generated. Then, for each realization, a simple optimization procedure is performed to maximize the trigger criterion V_{TFC}^{Lim} and thereby minimize the use of tower feedback control. The fatigue life criterion is required to be fulfilled only with a certain probability, thus making the optimization problem chance constrained.³⁰ In line with the previous discussion, the margin of safety is taken as approximately 5%. It is computationally impractical to perform a lifetime fatigue analysis for each random field realization. Therefore, response surface methodology is employed in the Monte Carlo analysis. In order to construct the response surfaces, lifetime fatigue analyses are carried out for selected quantiles in the distribution of the natural period. Furthermore, the analysis considers both a one-to-one and an uncertain relationship between the estimated natural period and the predicted fatigue life of the support structure. The one-to-one correspondence should be interpreted as an idealized situation. In reality, there is still uncertainty regarding the support structure's fatigue life when the post-installation controls adaptation is performed. Most of this uncertainty was present also in the pre-installation prediction of the fatigue life and need not be accounted for. The use of acceleration data to estimate the natural periods introduces uncertainty that was previously not present and should hence be taken into account. The uncertain natural period estimate \hat{T}_Δ is modeled as normally distributed with mean given by the true natural period T_Δ , such that

$$\hat{T}_1 = T_1 + \epsilon, \quad \epsilon \sim \mathcal{N}(0, \hat{\eta}\sigma_{T_1}). \quad (11)$$

It is useful to express the post-installation estimation uncertainty as a function of the pre-installation uncertainty in the natural period. The standard deviation of the estimation error ϵ is therefore given by the standard deviation of the natural period σ_{T_Δ} multiplied by a factor $\hat{\eta}$.

Figure 7 presents the outcomes of the post-installation adaptation of tower feedback control when there is perfect knowledge of the true natural period ($\hat{\eta} = 0.0$). In the idealized situation, there is approximately a 60% probability of tower feedback control being used ($V_{TFC}^{Lim} < 26$ [m/s]) and a 5% probability of tower feedback control being used to the full extent possible ($V_{TFC}^{Lim} = 4$ [m/s]). Natural periods in between the 40%- and 95%-quantiles lead to varying degree of tower feedback control, and maximum utilization of the support structure's fatigue life ($D_{Max}^{20-year} = 1.0$). Clearly, as a result of the post-installation controls adaptation, the support structures' fatigue life is equalized over a range of natural periods. This admits the possibility of decommissioning the turbines across the wind farm at the same time without wasting structural reserves. In effect, the two-stage controls adaptation can also be viewed as a means of reducing conservatism in the design of the support structures.

Figure 8 presents the outcomes of the post-installation adaptation of tower feedback control when there is uncertainty about the true natural period. As expected, estimation uncertainty lead to an increase in the incidence of tower feedback control. At the present level of uncertainty, there are instances of tower feedback control across the whole range of natural periods. Nevertheless, the overall degree to which tower feedback control is being used decreases with decreasing natural period. On average, a significant reduction in adverse side-effects is therefore

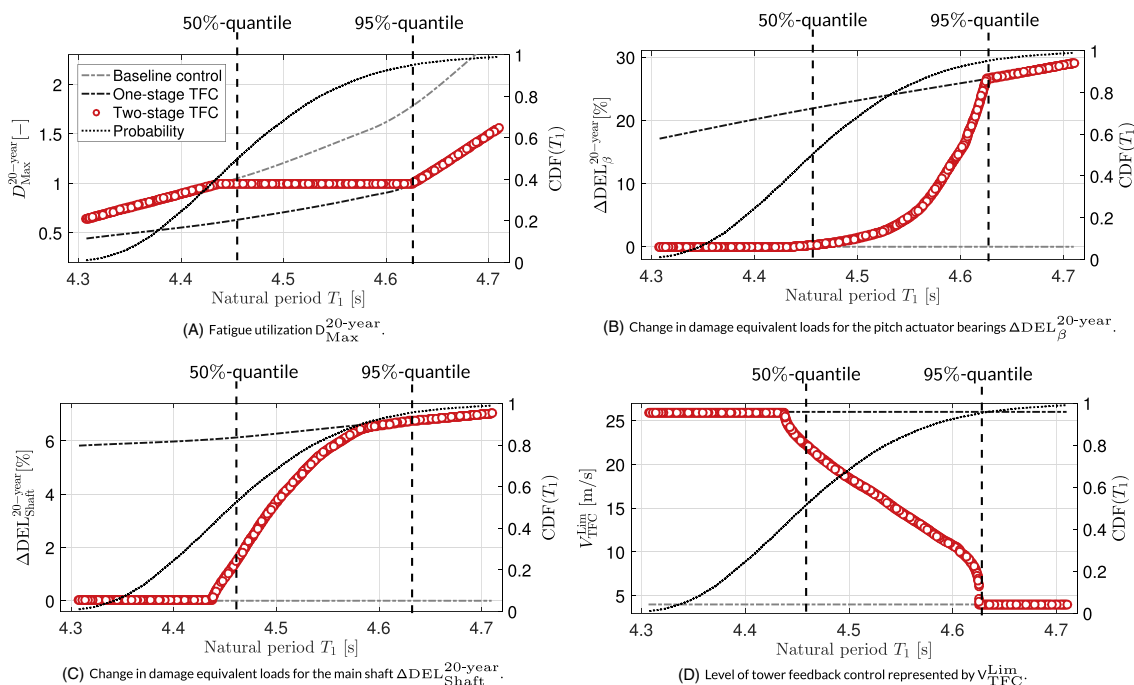


FIGURE 7 Monte Carlo outcomes of the two-stage adaptation of tower feedback control (TFC) when there is perfect knowledge of the true natural period ($\hat{\eta} = 0.0$). The results are generated from 10 000 random field realizations

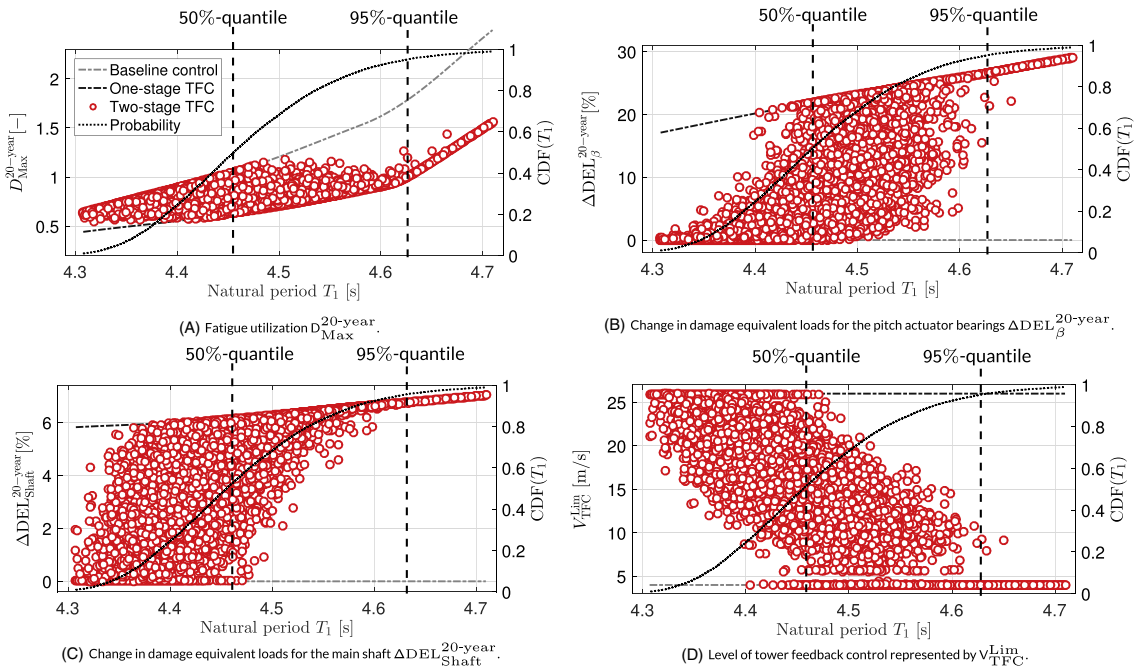


FIGURE 8 Monte Carlo outcomes of the two-stage adaptation of tower feedback control (TFC) when there is uncertainty about the true natural period ($\hat{\eta} = 0.5$). The results are generated from 10 000 random field realizations

TABLE 6 Probabilistic outcome of the two-stage adaptation of tower feedback control

Case Description	$\Delta DEL_{\beta}^{20\text{-year}}, \%$	$\Delta DEL_{\text{Shaft}}^{20\text{-year}}, \%$	$P[V_{\text{TFC}}^{\text{Lim}} = 4], \%$	$P[V_{\text{TFC}}^{\text{Lim}} < 26], \%$	$P[D_{\text{Max}}^{20\text{-year}} > 1.0], \%$
Conventional one-stage adaptation	22.1	6.2	100.0	100.0	5.0
Two-stage adaptation $\hat{\eta} = 0.0$	3.0	2.3	5.0	58.4	5.0
Two-stage adaptation $\hat{\eta} = 0.25$	5.4	3.3	10.6	76.3	6.2
Two-stage adaptation $\hat{\eta} = 0.5$	8.8	4.4	22.0	88.2	6.2
Two-stage adaptation $\hat{\eta} = 0.75$	12.2	5.0	36.0	92.7	6.2
Two-stage adaptation $\hat{\eta} = 1.0$	15.1	5.4	52.8	94.4	6.2

Note. The average change in damage equivalent loads for the pitch actuator bearings and main shaft are denoted as $\Delta DEL_{\beta}^{20\text{-year}}$ and $\Delta DEL_{\text{Shaft}}^{20\text{-year}}$, respectively. Further, $P[V_{\text{TFC}}^{\text{Lim}} < 26]$ is the probability of tower feedback control being used and $P[V_{\text{TFC}}^{\text{Lim}} = 26]$ is the probability of it being used to the full extent possible. The probability of the maximum fatigue utilization being exceeded $P[D_{\text{Max}}^{20\text{-year}} > 1.0]$ can be interpreted as the probability of failure. The results are generated from 10 000 random field realizations.

expected even in the presence of estimation uncertainty. Notably, there are very few instances of tower feedback control not being used at maximum capacity for natural periods above the 95th-quantile.

Table 6 presents the probabilistic outcome of the two-stage adaptation of tower feedback control under varying levels of estimation uncertainty. Furthermore, the average increase in the pitch bearings' and main shaft's fatigue loads is presented as a function of the level of estimation uncertainty in Figure 9. In all cases, the post-installation controls adaptation leads to a significant reduction in the adverse side-effects of tower feedback control. The proposed methodology adds complexity to the turbines' control and sensor systems, and to the structural design process in general. A substantial reduction in the adverse side-effects of tower feedback control should be demonstrated in order to justify this added complexity. Arguably, even when the estimation uncertainty is on the order of the pre-installation uncertainty in the natural period ($\hat{\eta} = 1.0$), the post-installation controls adaptation leads to a large reduction in adverse side-effects, particularly for the pitch actuators. Of course, this result depends on how the different components are prioritized in the second stage controls adaptation.

7 | TWO-STAGE ADAPTATION OF A CONTROL STRATEGY FOR SERVICEABILITY LOAD REDUCTION

The two-stage adaptation of a control strategy capable of increasing the serviceability capacity of support structures is analyzed in the following. First, the lifetime effects of the adopted control strategy are analysed. Then, the procedure for the second stage controls adaptation is established. Finally, the probabilistic outcome of the two-stage controls adaptation is analyzed.

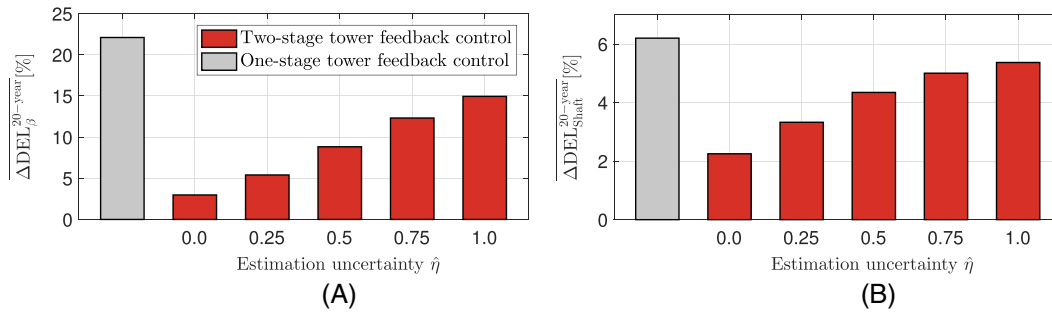


FIGURE 9 Probabilistic outcome of the two-stage adaptation of tower feedback control. The average change in damage equivalent loads for the pitch actuator bearings and main shaft are denoted as $\Delta\text{DEL}_{\beta}^{20\text{-year}}$ and $\Delta\text{DEL}_{\text{Shaft}}^{20\text{-year}}$, respectively. The results are generated from 10 000 random field realizations

7.1 | First-stage controls adaptation

The first stage adaptation of a control strategy capable of increasing the serviceability capacity of support structures is performed in this section. Unlike fatigue-reducing control measures, methodology for improving serviceability is not much discussed in the literature on wind turbine control. While the support structures' fatigue life is governed by normal loading conditions, their serviceability capacities are determined by the ability to resist tilting under certain loading conditions. Control measures for improving serviceability can therefore be targeted more directly at the design-driving loads. Reducing the maximum aerodynamic thrust via so-called peak shaving is effective for reducing wind-induced overturning moments in near-rated conditions.⁶³ Thus, peak shaving provides a means of increasing the serviceability capacity of support structures.

Peak shaving is achieved by pitching to feather to reduce the rotor's aerodynamic efficiency in near-rated conditions. Implementing such a control strategy is fairly straightforward and requires only a simple mapping from a selected peak shaving parameter to the rotor's collective pitch angle.⁶³ In the present work, the power output P_{Out} is taken as the peak shaving parameter and the demanded pitch angle β_{PS} is calculated using the following relationship:

$$\beta_{\text{PS}} = \max(\min(\beta(P_{\text{Out}}; \beta_{\text{PS}}^{\text{Max}}), \beta_{\text{PS}}^{\text{Max}}), 0), \quad \beta(P_{\text{Out}}; \beta_{\text{PS}}^{\text{Max}}) = a(\beta_{\text{PS}}^{\text{Max}})P_{\text{Out}} + b(\beta_{\text{PS}}^{\text{Max}}). \quad (12)$$

The level of peak shaving depends on the prescribed pitch angle $\beta_{\text{PS}}^{\text{Max}}$ at which rated power is reached. Within the peak shaving region, the pitch angle is adjusted as a linear function of the power output. For a given level of peak shaving, the constants a and b are selected with the aim of minimizing adverse side-effects. A more favorable trade-off between load reduction and adverse side-effects can be achieved by using a higher order peak shaving method, such as those described by Perley et al.⁶³ However, given the relatively low potential for improvement, further optimization efforts are considered outside the scope of this paper.

Since peak shaving is achieved by reducing the rotor's aerodynamic efficiency, it unavoidably leads to power losses that may significantly reduce the lifetime energy yield. Support structures are typically reported to contribute approximately 20% to the cost of offshore wind energy.^{2,61} Thus, any percentage loss of power production revenue must be offset by a five-fold percentage reduction in the cost of support structures. The lifetime energy yield is estimated from time histories of power output obtained from aero-hydro-servo-elastic simulations. First, the mean wind speed data are grouped into intervals of 1 [m/s]. Then, for each interval, simulations of 3600 [s] duration are performed, taking the midpoint of the interval as the mean wind speed. Turbulence and wind shear are accounted for in accordance with IEC 61400-1,⁵¹ assuming Class B normal turbulence conditions. The negligible effect of wave loads on the power output is not accounted for in the analysis.

Table 7 presents the result of the first stage adaptation of peak shaving. The selected level of peak shaving leads to a significant increase in the serviceability capacity. No strategies have been adopted to increase the serviceability capacity in near-cut-out conditions. The near-cut-out serviceability capacity is therefore taken as the target capacity in near-rated conditions. Furthermore, a normalization factor is applied to the results in order to achieve the target serviceability utilization ($\theta_{\text{Max}}^{1\text{-year}} = 1$) only if peak shaving is used. As expected, peak shaving reduces the lifetime energy yield. At the present level of peak shaving ($\beta_{\text{PS}}^{\text{Max}} = 6^\circ$), the cost savings enabled by increasing the serviceability capacity are unlikely to offset the loss of power production revenue.

Figure 10 presents the effect of the applied peak shaving strategy on selected wind turbine parameters as a function of wind speed. It is apparent that peak shaving reduces the maximum steady-state thrust at the expense of power losses. Although these power losses are limited to a relatively small range of wind speeds, they occur in wind conditions which contribute significantly to the lifetime energy yield. Their effect in terms of lost power production is therefore considerable.

TABLE 7 Results for the first stage adaptation of peak shaving to increase the support structure's serviceability capacity

Controller Adaptation	Serviceability Utilization			Adverse Side Effects
	$\theta_{\text{Rated}}^{1\text{-year}}$, -	$\theta_{\text{Cut-out}}^{1\text{-year}}$, -	$\Delta\theta_{\text{Max}}^{1\text{-year}}$, %	$\Delta P_{\text{Out}}^{20\text{-year}}$, %
Baseline control	1.6	1.0	0.0	0.0
Peak shaving	1.0	1.0	-37.4	-2.1

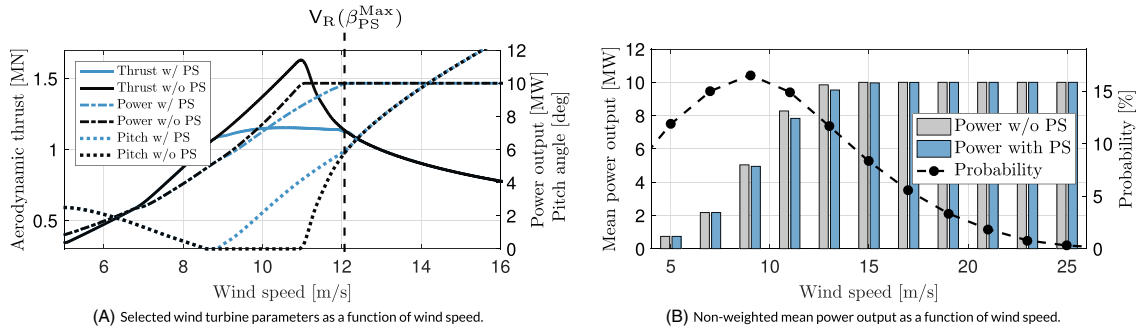


FIGURE 10 The effect of the applied peak shaving (PS) strategy on selected wind turbine parameters as a function of wind speed. The wind speed at which rated power is reached $V_R(\beta_{PS}^{Max})$ with the applied level of peak shaving ($\beta_{PS}^{Max} = 6^\circ$) is indicated

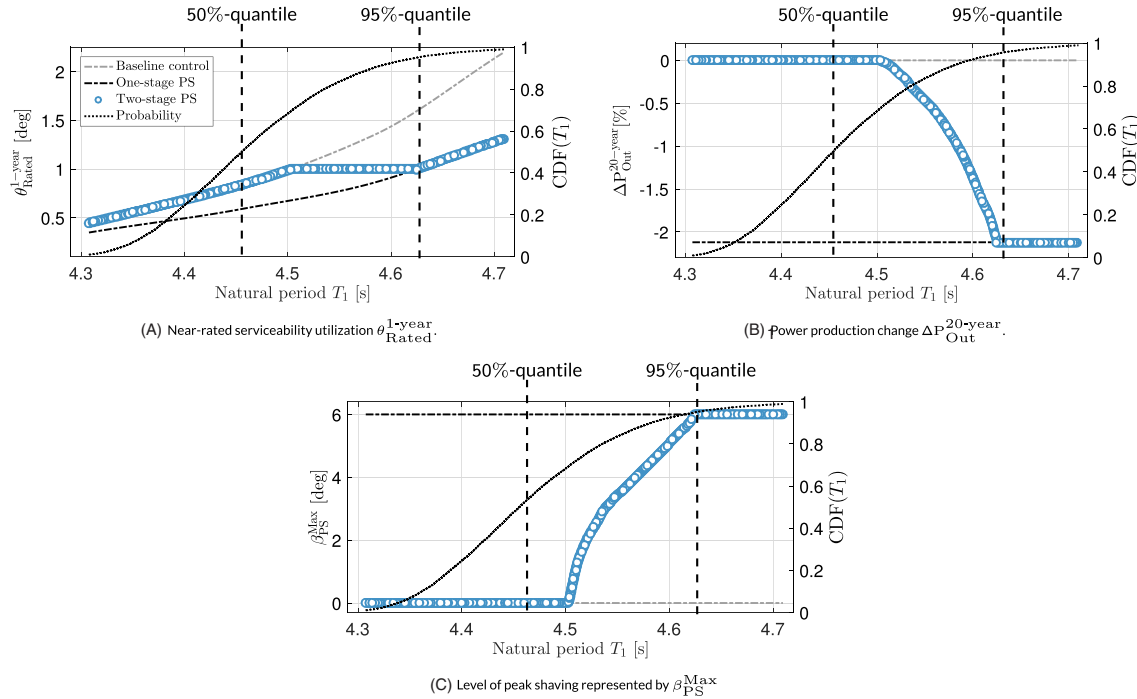


FIGURE 11 Trade-off between reduction of serviceability utilization in rated conditions $\Delta\theta_{Rated}^{1-year}$ and power production change $\Delta P_{Out}^{20-year}$. Results are presented for characteristic soil properties corresponding to 1%- and 99%-quantiles in the distribution of the natural period T_Δ

7.2 | Second-stage controls adaptation

The procedure for the second stage adaptation of peak shaving is established in the following. For a given outcome of the site-specific soil conditions, the required level of serviceability load reduction can be achieved by straightforward adjustment of β_{PS}^{Max} . The result is, of course, a trade-off between serviceability load reduction and power production.

The trade-off between reduction of serviceability utilization in rated conditions and lifetime energy yield is presented in Figure 11. Increasing the peak shaving yields diminishing returns in terms of serviceability utilization. There is clearly a threshold beyond which increasing the serviceability capacity cannot justify the added power losses. Like tower feedback control, peak shaving is most effective when the soil-pile stiffness is low. Due to the nonlinear behavior of the soil, reducing the overturning moment has a greater effect on the tilt angle when the soil undergoes large deformations. Accordingly, the difference between the serviceability utilization in cut-out and rated conditions without peak shaving decreases as a function of soil-pile stiffness. Notably, the cost of increasing the near-rated serviceability capacity to eliminate this difference appears not to be very sensitive to variations the soil conditions. It is therefore reasonable to apply the same maximum level of peak shaving ($\beta_{PS}^{Max} = 6^\circ$) in the first- and second-stage controls adaptation.

7.3 | Probabilistic outcome of the two-stage controls adaptation

The probabilistic outcome of the two-stage adaptation of peak shaving is analyzed in this section. The procedure for calculating the probabilistic outcome of the post-installation adaptation of peak shaving is similar to that of tower feedback control. First, a set of random field realizations is generated. Then, for each realization, an optimization procedure is performed to minimize the level of peak shaving and thereby the associated power losses. Response surfaces are constructed by carrying out serviceability analyses under different levels of peak shaving for selected

quantiles in the distribution of the natural period. Uncertainty in the estimates of the natural period is modeled following the approach proposed in Section 6.3.

The outcomes of the post-installation adaptation of peak shaving when there is perfect knowledge of the true natural period is presented in Figure 12. As expected, maximum peak shaving ($\beta_{Max}^{PS} = 6^\circ$) is employed only if the natural period is at or above its 95%-quantile. Furthermore, the natural period below which peak shaving is not used at all ($\beta_{Max}^{PS} = 0^\circ$) falls at approximately the 70%-quantile. Instances of natural periods in between these quantiles lead to varying degree of of peak shaving, and maximum utilization of the support structure's serviceability capacity ($\theta_{Max}^{1-year} = 1.0$). Figure 13 presents the outcomes of the post-installation adaptation of peak shaving when there is uncertainty about the true natural period. Except for a few instances, maximum peak shaving is employed consistently for natural periods above the 95%-quantile. At the present level of uncertainty, the natural period below which there are no instances of peak shaving is reduced to approximately the 5%-quantile. Hence, the total incidence of peak shaving and its associated power losses is significantly increased compared with the idealized situation without estimation uncertainty.

Table 8 presents the probabilistic outcome of the two-stage adaptation of peak shaving under varying levels of estimation uncertainty. Furthermore, the mean change in the lifetime energy yield is presented as a function of the level of uncertainty in Figure 14. The post-installation controls adaptation leads to a substantial reduction of the average power production losses. As expected, the incidence of peak shaving and the mean change in the lifetime energy yield increases with increasing estimation uncertainty. Although the average power losses are reduced, they might still be too large to be offset by the cost savings enabled by peak shaving. Nevertheless, the results highlight an important implication of the proposed methodology. Since the adverse side-effects on average is reduced by up to an order of magnitude, a post-installation adaptation of load reducing controls could enable the use of control strategies that were previously not economically viable. At least, it would enable using control strategies to a fuller extent of their capabilities.

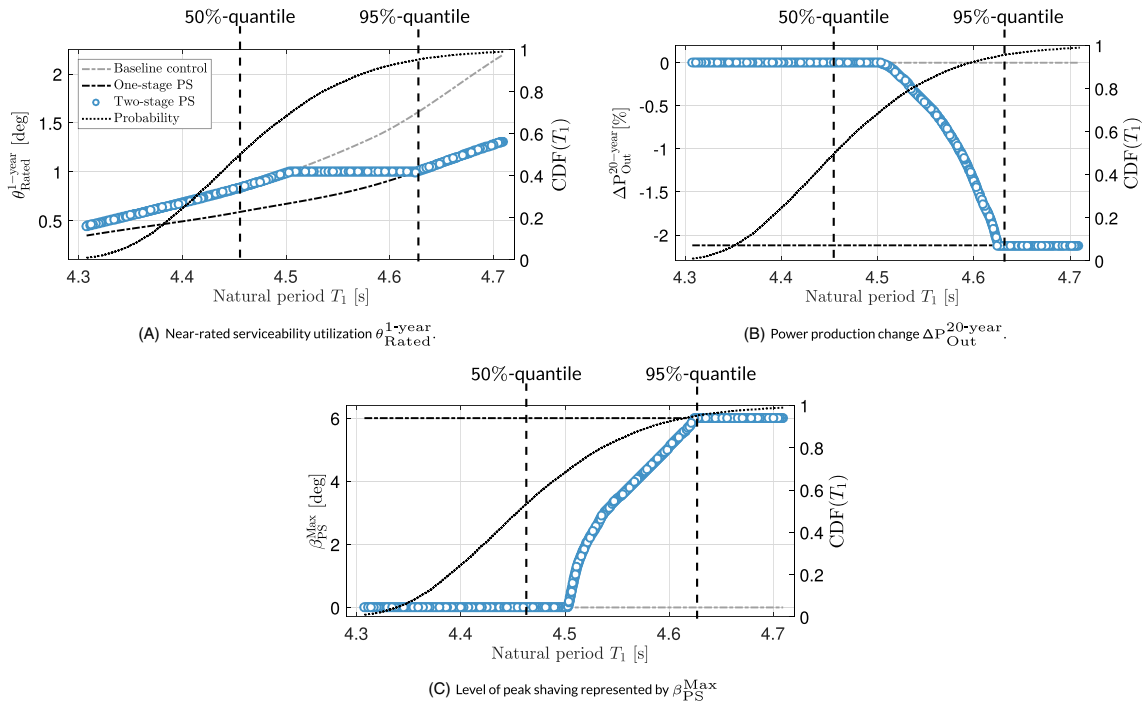


FIGURE 12 Monte Carlo outcomes of the two-stage adaptation of peak shaving (PS) when there is perfect knowledge of the true natural period ($\hat{\eta} = 0.0$). The results are generated from 10 000 random field realizations

TABLE 8 The probabilistic outcome of the two-stage adaptation of peak shaving

Case Description	$\Delta P_{Out}^{20-year}$, %	$[\beta_{Max}^{PS} = 6^\circ]$, %	$P[\beta_{Max}^{PS} > 0^\circ]$, %	$P[\theta_{Rated}^{1-year} > 1.0]$, %
One-stage adaptation	-2.1	100.0	100.0	5.0
Two-stage adaptation $\hat{\eta} = 0.0$	-0.2	5.0	30.4	5.0
Two-stage adaptation $\hat{\eta} = 0.25$	-0.4	11.0	47.8	5.5
Two-stage adaptation $\hat{\eta} = 0.5$	-0.8	22.3	66.5	5.5
Two-stage adaptation $\hat{\eta} = 0.75$	-1.1	37.8	79.4	5.5
Two-stage adaptation $\hat{\eta} = 1.0$	-1.4	52.5	86.0	5.5

Note. The average change in the lifetime energy yield is denoted as $\Delta P_{Out}^{20-year}$. Further, $P[\beta_{Max}^{PS} > 0]$ is the probability of peak shaving being used and $P[\beta_{Max}^{PS} = 6]$ is the probability of it being used to the full extent possible. The probability of the maximum serviceability utilization being exceeded $P[\theta_{Rated}^{1-year} > 1.0]$ can be interpreted as the probability of failure. The results are generated from 10 000 random field realizations.

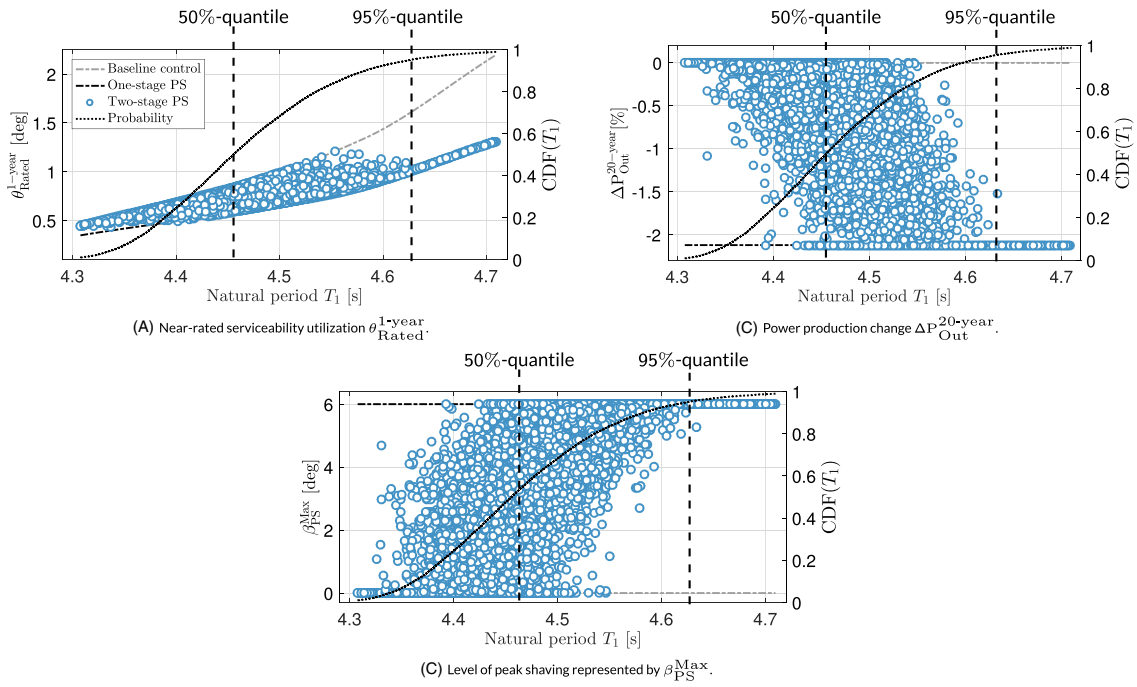


FIGURE 13 Monte Carlo outcomes of the two-stage adaptation of peak shaving (PS) when there is uncertainty about the true natural period ($\hat{\eta} = 0.5$). The results are generated from 10 000 random field realizations

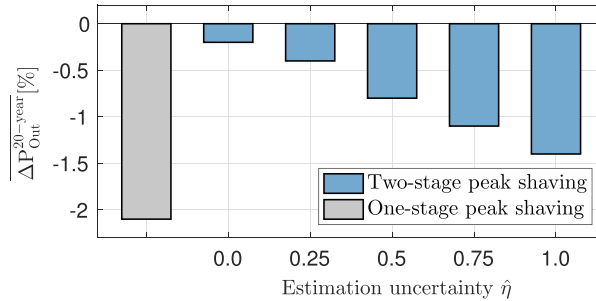


FIGURE 14 Probabilistic outcome of the two-stage adaptation of tower feedback control. The average change in power production is denoted as $\Delta P_{\text{Out}}^{20\text{-year}}$. The results are generated from 10 000 random field realizations

8 | CONCLUSIONS

In this paper, the potential of making turbine-specific adjustments to the wind turbines' control systems after their installation was analyzed. The analysis considered the structural design of a 10 MW monopile offshore wind turbine under uncertainties in the geotechnical properties. An adaptation of the wind turbines' control system in two stages was proposed. In the first stage, carried out during the structural design process, control strategies were adopted to reduce the support structure's load effects. In this stage, the structural capacities were uncertain due to inherent variability in the site-specific soil properties. Under the assumption that the true structural capacities could be estimated once the turbines were installed, the second stage controls adaptation was carried out. The objective of the second stage was to minimize the use of the control strategies adopted in the first stage, while still adhering to the required level of structural safety. Two control strategies were considered in separate analyses. In both analyses, the two-stage controls adaptation was analyzed using response surface methodology and Monte Carlo simulations. The response surfaces were constructed from results obtained via aero-hydro-servo-elastic simulations.

The first control strategy under consideration was tower feedback control to increase the support structure's fatigue life. While effective, the additional pitch activity led to increased fatigue loads for the pitch actuators and main shaft. As a procedure for the post-installation controls adaptation, it was proposed to use event-triggered tower feedback control. Tradespaces revealed that the best choice of trigger criteria depended on the priority of the adversely affected components. Nevertheless, since some general patterns were observed, it was found reasonable to define a single set of trigger criteria independent of the site-specific soil conditions. Monte Carlo simulation of the two-stage controls adaptation showed that the incidence of tower feedback control and its adverse side-effects was significantly reduced as a result of the post-installation controls adaptation.

The second control strategy under consideration was peak shaving to increase the support structure's serviceability capacity. Peak shaving was effective for improving serviceability, but led to significant power losses. It was found unlikely that the cost savings enabled by the applied peak shaving strategy could offset the loss of power production revenue without further actions being taken. Further, the trade-off between serviceability load reduction and power production was analyzed in connection with the second-stage controls adaptation. Increasing the peak shaving was found to yield diminishing returns in terms of serviceability utilization. As expected, Monte Carlo simulation showed that the post-installation controls adaptation led to a significant reduction in the incidence of peak shaving and its associated power losses.

ACKNOWLEDGMENTS

This work has been carried out at the Centre for Autonomous Marine Operations and Systems (NTNU AMOS). The Norwegian Research Council is acknowledged as the main sponsor of NTNU AMOS. This work was supported by the Research Council of Norway through the Centres of Excellence funding scheme, Project number 223254-NTNU AMOS.

ORCID

Emil Smilden  <https://orcid.org/0000-0001-8547-9353>

Erin E. Bachynski  <https://orcid.org/0000-0002-1471-8254>

REFERENCES

1. Ho A, Mbistrova A, Corbetta G, Pineda I, Ruby K. The European offshore wind industry-key trends and statistics. *Report. Brussels: European Wind Energy Association*. 2016;.
2. Fischer TA. *Mitigation of Aerodynamic and Hydrodynamic Induced Loads of Offshore Wind Turbines*. Shaker. University of Stuttgart; 2012.
3. Hooft EL, Schaak P, Van Engelen TG. Wind turbine control algorithms. *DOWEC project-DOWEC-F1W1-EH-03-094/0, Task-3 report*. 2003;.
4. Bossanyi EA. Wind turbine control for load reduction. *Wind Energy*. 2003;6(3):229-244.
5. Bossanyi EA, Ramtharan G, Savini B. The importance of control in wind turbine design and loading. In: *2009 17th Mediterranean Conference on Control and Automation*. IEEE; 2009:1269-1274.
6. Boris F, Martin S. A Survey on Control mMethods for the Mitigation of Tower Loads. *Fraunhofer-Institute for Wind Energy and Energy Systems Technology, IWES Project report 01/104256*. 2013.
7. Smilden E, Bachynski EE, Sørensen AJ, Amdahl J. Site-specific controller design for monopile offshore wind turbines. *Mar Struct*. 2018;61:503-523.
8. Carswell W, Arwade SR, DeGroot DJ, Lackner MA. Soil-structure reliability of offshore wind turbine monopile foundations. *Wind energy*. 2015;18(3):483-498.
9. Carswell W, Arwade SR, DeGroot DJ, Myers AT. Natural frequency degradation and permanent accumulated rotation for offshore wind turbine monopiles in clay. *Renew Energy*. 2016;97:319-330.
10. Andersen LV, Vahdatirad MJ, Sichani MT, Sørensen JD. Natural frequencies of wind turbines on monopile foundations in clayey soils—A probabilistic approach. *Computers and Geotechnics*. 2012;43:1-11.
11. Mads D, Mehdi B, Andersen LV, Ibsen LB. Assessment of the dynamic behaviour of saturated soil subjected to cyclic loading from offshore monopile wind turbine foundations. *Comput Geotech*. 2014;61:116-126.
12. Mads D, Andersen LV, Ibsen LB, Toft HS, Sørensen JD. A probabilistic analysis of the dynamic response of monopile foundations: Soil variability and its consequences. *Probabilistic Eng Mech*. 2015;41:46-59.
13. Domenico L, Subhamoy B, Wood DM. Dynamic soil-structure interaction of monopile supported wind turbines in cohesive soil. *Soil Dyn Earthq Eng*. 2013;49:165-180.
14. Subhamoy B. Challenges in design of foundations for offshore wind turbines. *Eng Technol Ref*. 2014;1(1):1-9.
15. Arany L, Bhattacharya S, Macdonald J, Hogan SJ. Simplified critical mudline bending moment spectra of offshore wind turbine support structures. *Wind Energy*. 2015;18(12):2171-2197.
16. Arany L, Bhattacharya S, Macdonald J, Hogan SJ. Design of monopiles for offshore wind turbines in 10 steps. *Soil Dyn Earthq Eng*. 2017;92:126-152.
17. Arany L, Bhattacharya S, Macdonald JH, Hogan SJ. A critical review of serviceability limit state requirements for monopile foundations of offshore wind turbines. In: *Offshore Technology Conference*; 2015.
18. Seidel M, Voormeeren S, Steen JB. State-of-the-art design processes for offshore wind turbine support structures. *Stahlbau*. 2016;85(9):583-590.
19. Martinez-Luengo M, Kolios A, Wang L. Structural health monitoring of offshore wind turbines: A review through the Statistical Pattern Recognition Paradigm. *Renew Sustain Energy Rev*. 2016;64:91-105.
20. Gomez HC, Gur T, Dolan D. Structural condition assessment of offshore wind turbine monopile foundations using vibration monitoring data. In: *Nondestructive Characterization for Composite Materials, Aerospace Engineering, Civil Infrastructure, and Homeland Security 2013*. International Society for Optics and Photonics; 2013:86940B.
21. Smarsly K, Hartmann D, Law KH. A computational framework for life-cycle management of wind turbines incorporating structural health monitoring. *Struct Health Monit*. 2013;12(4):359-376.
22. Devriendt C, Guillaume P. Identification of modal parameters from transmissibility measurements. *J Sound Vib*. 2008;314(1-2):343-356.
23. Devriendt C, Jordeaens PJ, De Sitter G, Guillaume P. Damping estimation of an offshore wind turbine on a monopile foundation. *IET Renew Power Gener*. 2013;7(4):401-412.
24. Devriendt C, Magalhães F, Weijtjens W, De Sitter G, Cunha Á, Guillaume P. Structural health monitoring of offshore wind turbines using automated operational modal analysis. *Struct Health Monit*. 2014;13(6):644-659.
25. Weijtjens W, Verbelen T, De Sitter G, Devriendt C. Foundation structural health monitoring of an offshore wind turbine—a full-scale case study. *Struct Health Monit*. 2016;15(4):389-402.

26. Damgaard M, Ibsen LB, Andersen LV, Andersen LK. Cross-wind modal properties of offshore wind turbines identified by full scale testing. *J Wind Eng Ind Aerodyn*. 2013;116:94-108.
27. Hansen MH, Thomsen K, Fuglsang P, Knudsen T. Two methods for estimating aeroelastic damping of operational wind turbine modes from experiments. *Wind Energy*. 2006;9(1-2):179-191.
28. Fischer T, Vries W, Rainey P, Schmidt B, Argyriadis K, Kühn M. Offshore support structure optimization by means of integrated design and controls. *Wind Energy*. 2012;15(1):99-117.
29. King AJ, Wallace SW. *Modeling with Stochastic Programming*. Springer Science & Business Media; 2012.
30. Seidel M. Design of support structures for offshore wind turbines—Interfaces between project owner, turbine manufacturer, authorities and designer. *Stahlbau*. 2010;79(9):631-636.
31. IEC 61400-3. Wind Turbines—Part 3: Design Requirements for Offshore Wind Turbines. *Design standard*. 2009.
32. Phoon KK, Kulhawy FH. Characterization of geotechnical variability. *Can Geotech J*. 1999;36(4):612-624.
33. Phoon KK, Kulhawy FH. Evaluation of geotechnical property variability. *Can Geotech J*. 1999;36(4):625-639.
34. Vanmarcke EH. Probabilistic modeling of soil profiles. *J Geotech Eng Div*. 1977;103(11):1227-1246.
35. Schneider HR, Schneider MA. Dealing with uncertainties in EC7 with emphasis on determination of characteristic soil properties. In: Arnold P, Fenton GA, Hicks MA, Schweckendiek T, eds. *Modern Geotechnical Design Codes of Practice*. Rotterdam, the Netherlands: IOS Press; 2012:87-101.
36. Prendergast LJ, Reale C, Gavin K. Probabilistic examination of the change in eigenfrequencies of an offshore wind turbine under progressive scour incorporating soil spatial variability. *Mar Struct*. 2018;57:87-104.
37. Ronold KO. Characteristic soil strength for axial pile capacity and its estimation with confidence for offshore applications. *Struct Saf*. 2016;63:81-89.
38. API, RP. 2GEO (2011). *Recommended Practice for Geotechnical Foundation Design Consideration*. 2011;.
39. Veritas DN. *DNV-OS-J101 Offshore Standard: Design of Offshore Wind Turbine Structures*. Høvik, Norway: DNV AS; 2014.
40. Murchison JM, O'Neill MW. Evaluation of ϕ relationships in cohesionless soils. In: *Analysis and design of pile foundations*. ASCE; 1984:174-191.
41. Matlock H. Correlations for design of laterally loaded piles in soft clay. *Offshore technology in civil engineering's hall of fame papers from the early years*. 1970;77-94.
42. Reese LC, Welch RC. Lateral loading of deep foundations in stiff clay. *J Geotech Geoenviron Eng ASCE*. 1975;101(7):633-649.
43. Bak C, Zahle F, Bitsche R, et al. Description of the DTU 10 MW reference wind turbine. *DTU Wind Energy Report-I-0092*. 2013;.
44. Hansen MH, Henriksen LC. Basic DTU Wind Energy Controller. DTU Wind Energy; 2013.
45. Bachynski EE, Ormberg H. Hydrodynamic Modeling of Large-Diameter Bottom-Fixed Offshore Wind Turbines. In: *ASME 2015 34th international conference on ocean, offshore and arctic engineering: V009T09A051*. American Society of Mechanical Engineers; 2015.
46. Ormberg H, Bachynski EE. Global analysis of floating wind turbines: Code development, model sensitivity and benchmark study. In: *The Twenty-second International Offshore and Polar Engineering Conference*. International Society of Offshore and Polar Engineers; 2012.
47. DNV GL. DNV-RP-C205. *Environmental conditions and environmental loads*. 2010.
48. Jonkman BJ *TurbSim user's guide*. 2009.
49. GL DNV. DNVGL-ST-0437: Loads and site conditions for offshore wind turbines. *DNV GL, Høvik, Norway*. 2016.
50. Reistad M, Breivik Ø, Haakenstad H, Aarnes OJ, Furevik BR, Bidlot JR. A high-resolution hindcast of wind and waves for the North Sea, the Norwegian Sea, and the Barents Sea. *J Geophys Res Oceans*. 2011;116(C5):1-18
51. International Electrotechnical Commission (IEC). IEC 61400-1: Wind turbines part 1: Design requirements. 2005.
52. Andersen LV, Sørensen JD, Kim SB, et al. Influence of Characteristic-Soil-Property-Estimation Approach on the Response of Monopiles for Offshore Wind Turbines. *J Ocean Wind Energy*. 2015;2(3):160-167.
53. Li Q, Gao Z, Moan T. Modified environmental contour method for predicting long-term extreme responses of bottom-fixed offshore wind turbines. *Mar Struct*. 2016;48:15-32.
54. Winterstein SR, Ude TC, Cornell CA, Bjerager P, Haver S. Environmental parameters for extreme response: Inverse FORM with omission factors. In: *Proceedings of the ICOSSAR-93*. Innsbruck, Austria; 1993:551-557.
55. Johannessen K, Meling TS, Hayer S. Joint distribution for wind and waves in the northern north sea. In: *The Eleventh International Offshore and Polar Engineering Conference*. International Society of Offshore and Polar Engineers; 2001.
56. Muskulus M, Schafhirt S. Reliability-based design of wind turbine support structures. In: *Proceedings of the Symposium on Reliability of Engineering System, Hangzhou, China*; 2015.
57. GL DNV. Statistical representation of soil data. *DNV-RP-C207*. 2012.
58. Smilden E, Bachynski EE, Sørensen AJ, Amdahl J. Wave Disturbance Rejection for Monopile Offshore Wind Turbines. *Wind Energy*. 2018;22(1):89-108.
59. DNV GL. OS-C101. *Design of Offshore Steel Structures*. 2011.
60. Horn JT, Bitner-Gregersen E, Krokstad JR, Leira BJ, Amdahl J. A new combination of conditional environmental distributions. *Appl Ocean Res*. 2018;73:17-26.
61. Shrestha B, Kühn M. Tailoring the Employment of Offshore Wind Turbine Support Structure Load Mitigation Controllers. *J Phys Conf Ser*. 2016;753(5):1-10.
62. Shrestha B, Kühn M. Adaptation of Controller Concepts for Support Structure Load Mitigation of Offshore Wind Turbines. *Energy Procedia*. 2016;94:241-248.
63. Perley TF, Busbey BC, Gerber BS. System and methods for determining pitch angles for a wind turbine during peak shaving. US Patent App. 13/359,837; 2013.